J Solid State Electrochem (1998) 2: 291–298

ORIGINAL PAPER

Chung-Liang Chang · Tai-Cheng Lee · Ta-Jen Huang

Oxygen reduction mechanism and performance of $Y_1Ba_2Cu_3O_{7-\delta}$ as a cathode material in a high-temperature solid-oxide fuel cell

Received: 28 October 1997 / Accepted: 16 January 1998

Abstract The high-Tc $Y_1Ba_2Cu_3O_{7-\delta}$ superconductor with oxygen ion vacancies was employed as the cathode for a high-temperature solid-oxide fuel cell (SOFC). The cathodic current-overpotential characteristics were studied in the temperature range from 500 to 800 °C and the oxygen pressure range from 10^{-4} to 0.21 atm. The delocalization of the triple-phase boundary and the oxygen reduction mechanism were identified. The delocalized triple-phase boundary of $Y_1Ba_2Cu_3O_{7-\delta}$ improves the cathodic polarization in SOFCs. By using a mathematical simulation and a particular experimental design, the oxygen adsorption step in the oxygen reduction process was demonstrated to be rate limiting. A layer of strong oxygen-adsorption catalyst such as Pt or Ag coated on the $Y_1Ba_2Cu_3O_{7-\delta}$ electrode was found to be able to largely enhance the activity of oxygen reduction by improving the ability of oxygen to be adsorbed on the electrode surface.

Key words $Y_1Ba_2Cu_3O_{7-\delta}$ · Oxygen ion vacancy · Triple-phase boundary · Oxygen adsorption · SOFC

List of symbols

B_m:	mobility
C_O:	the concentration of the adsorbed oxygen atom
$C_{O_{(eq)}}$:	the concentration of the adsorbed oxygen atom at thermodynamic equilibrium
C_{Oo^x}:	the concentration of the oxygen ion in vacancies
$C_{Oo_{(eq)}}$:	the concentration of the oxygen ion in vacancies at thermodynamic equilibrium
E_{eq}:	open-circuit potential
$E^{o'}$:	formal potential
F:	Faraday constant
f:	F/RT
I:	current
I_o:	exchange current
K:	dissociation equilibrium constant
k_a:	adsorption constant
L:	electrode thickness
n:	the number of electrons
O:	oxygen atom
$O_{O^x_{(YBCO)}}$:	oxygen ion in an oxygen vacancy of YBCO
$O_{O^x_{(YSZ)}}$:	oxygen ion in an oxygen vacancy of YSZ
$O^*_{(s)}$:	oxygen adsorbed on electrode surface
$O^*_{(v)}$:	oxygen adsorbed on oxygen vacancy
P_{O_2}:	oxygen pressure
R:	gas constant
r_a:	adsorption rate
T:	temperature
T_c:	critical temperature
$V_{\ddot{O}}$:	oxygen vacancy
x:	position in electrode
z:	the valency of the oxygen ion
α:	transfer coefficient
η:	overpotential
ρ:	charge density
ϕ:	electric potential
ε_o:	dielectric constant
θ_O:	coverage of oxygen atom
θ_{O_2}:	coverage of oxygen molecule
*:	unoccupied active site

C.-L. Chang · T.-C. Lee · T.-J. Huang (✉)
Department of Chemical Engineering, National Tsing Hua University, Hsinchu, Taiwan 300, Republic of China
Tel.: +886-3-5716260; Fax: +886-3-5717126

Introduction

In investigations of the high-temperature superconductors, it is well known that various properties and structures of Cu-based high-Tc $Y_1Ba_2Cu_3O_{7-\delta}$ superconductors are strongly dependent on the oxygen stoichiometry [1–3]. However, it is less well known that $Y_1Ba_2Cu_3O_{7-\delta}$ is also a fast ion conductor; at least

oxygen ion is able to diffuse rather readily through the bulk of the compound at a temperature as low as 300 °C [1, 4–6]. Hence, $Y_1Ba_2Cu_3O_{7-\delta}$ is a mixed conductor in which the oxygen ions and the electronic species are mobile.

An important advantage of using mixed-conductor electrodes in a high-temperature solid-oxide fuel cell (SOFC) is to spread the triple-phase boundaries, i.e., the electrochemical reaction sites. This leads to a delocalization of oxygen reduction from the electrode-electrolyte interface to the whole surface of the electrode [7]. At present, perovskite-type mixed conductors are the most widely used and studied SOFC cathodes [8–11]. However, the complex mechanism of oxygen reduction on these materials has not yet been clearly understood.

In this work, $Y_1Ba_2Cu_3O_{7-\delta}$ is employed as a cathode material of SOFCs. The performance of a high-temperature SOFC is dependent on whether the materials problems arising from the high operating temperature will be resolved. For example, the selection criteria for cathode materials must meet many physicochemical requirements, such as thermal and chemical stability in air, low vapor pressure and lack of chemical reactivity with the electrolyte. According to many investigations into the preparation and synthesis of the superconductor, $Y_1Ba_2Cu_3O_{7-\delta}$ meets these requirements [12, 13]. Hence, it could be an excellent candidate for the cathode in the SOFC system. The purpose of this article is to identify the oxygen reduction mechanism and the current-overpotential characteristics of $Y_1Ba_2Cu_3O_{7-\delta}$ used as a cathode. According to the cathodic behavior of $Y_1Ba_2Cu_3O_{7-\delta}$, a reaction mechanism of oxygen reduction was established and demonstrated by a mathematical simulation to be consistent with the experimental results.

Experimental

Materials

The experimental apparatus is shown in Fig. 1. Platinum leads are employed to make the electrical contact to the electrode material for the potential measurements, which are performed as described in [14]. The solid oxide electrolyte is a stabilized cubic 8 mol% Y_2O_3-ZrO_2 (YSZ, Zircoa, USA). Commercial $Y_1Ba_2Cu_3O_{7-\delta}$ powder (Seattle Specialty Ceramic, USA) was homogenized into a paste. The paste was then painted on YSZ and fired at 850 °C for 90 min in air to form the cathode. The Pt paste (Heraeus, USA) was painted on YSZ to form the reference and counter electrodes. This was then fired at 850 °C for 90 min in air. In addition, two specific arrangements of electrodes, Pt/$Y_1Ba_2Cu_3O_{7-\delta}$ and Ag/$Y_1Ba_2Cu_3O_{7-\delta}$, were employed to identify the mechanism of oxygen reduction on $Y_1Ba_2Cu_3O_{7-\delta}$. These were prepared by painting a layer of Pt paste or Ag paste (Johnson Matthey, UK) on the $Y_1Ba_2Cu_3O_{7-\delta}$ electrode, which was then fired at 850 °C for 90 min in air.

The surface area of the $Y_1Ba_2Cu_3O_{7-\delta}$ was measured by the physical adsorption technique of nitrogen condensation. The surface area of the $Y_1Ba_2Cu_3O_{7-\delta}$ is around 1 m^2/g as calculated from the Brunauer, Emmett, and Teller (BET) equation.

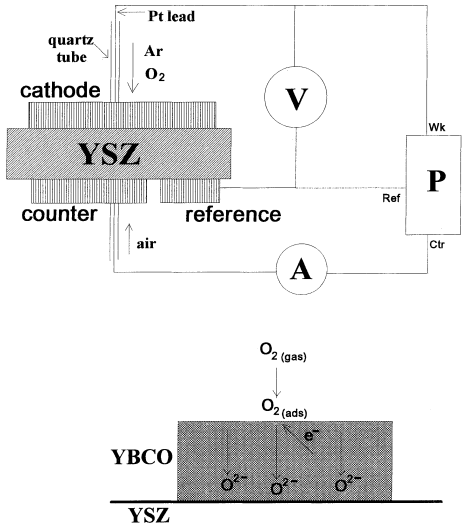

Fig. 1 Experimental apparatus and oxygen reduction pathway

Electrochemical measurement

In order to ascertain that $Y_1Ba_2Cu_3O_{7-\delta}$ was stable under the experimental conditions of temperature and oxygen partial pressure, an equilibrium potential of $Y_1Ba_2Cu_3O_{7-\delta}$ relative to Pt reference electrode was measured beforehand, which needed 2–3 h to obtain a stable value. The Pt reference electrode was exposed to air. The cathodic current-overpotential measurements were performed on a three-electrode cell configuration equipped with a potentiostat (Pine RDE4) and a digital multimeter (HP34401 A) with a 10 GΩ input resistance. To obtain reproducible data, every measurement of the cathode current vs overpotential needed 20 min to reach a steady value. The cathodic current-overpotential measurements were carried out at the temperature range from 500 to 800 °C and the oxygen partial pressure range from 10^{-4} to 0.21 atm.

Results and discussion

Cathodic current-overpotential characteristics

Comparison of $Y_1Ba_2Cu_3O_{7-\delta}$ and Pt

As can be seen from Fig. 2, at 500 °C and $P_{O_2} = 10^{-2}$ atm the $Y_1Ba_2Cu_3O_{7-\delta}$ electrode has a lower cathodic overpotential than that of the Pt electrode. This means that the use of $Y_1Ba_2Cu_3O_{7-\delta}$ as the cathode material can decrease the voltage loss of an SOFC due to cathodic polarization. As far as we are aware, this is the first report of any material which has a better cathodic performance than Pt at < 800 °C.

However, can be seen from Fig. 3, when the temperature is raised to 700 °C the cathodic overpotential of $Y_1Ba_2Cu_3O_{7-\delta}$ becomes larger than that of Pt. It should be noted that the reason for the overpotential range in Fig. 2 being smaller than that in Fig. 3 is because at the lower operating temperature of 500 °C (Fig. 2), the YSZ electrolyte has a larger ion-conductive resistance, so that the current and overpotential are limited to a smaller

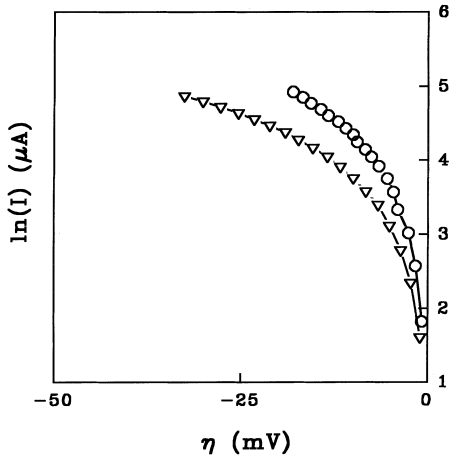

Fig. 2 Current-overpotential curves at 500 °C and $P_{O_2} = 10^{-2}$ atm; *circle symbol* YBCO electrode; *triangle symbol* Pt electrode

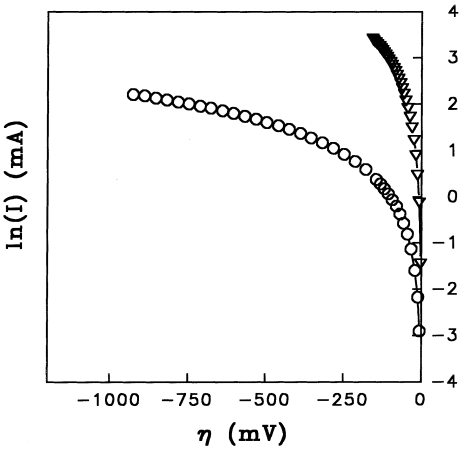

Fig. 3 Current-overpotential curves at 700 °C and $P_{O_2} = 10^{-2}$ atm; *circle symbol* YBCO electrode; *triangle symbol* Pt electrode

range to prevent it from destroying (blackening) the electrolyte structure. Pickett et al. [15] indicated that, at a constant oxygen pressure, the oxygen content in the $Y_1Ba_2Cu_3O_{7-\delta}$ lattice decreases as the temperature increases. Moreover, it was demonstrated [15, 16] that the reduction of the oxygen content in the $Y_1Ba_2Cu_3O_{7-\delta}$ lattice decreases the metallicity, and for large δ (>0.6), $Y_1Ba_2Cu_3O_{7-\delta}$ changes from a metallic state to a semiconductor state. At 500 °C and $P_{O_2} = 10^{-2}$ atm, the δ value is about 0.2 [17], and thus $Y_1Ba_2Cu_3O_{7-\delta}$ is kept in a metallic state. When the temperature is raised to 700 °C the δ value is raised to about 0.65, and thus the electrical property of $Y_1Ba_2Cu_3O_{7-\delta}$ changes to that of a semiconductor. According to the electronic band theory [18], the change of the electrical property from a metallic state to a semiconductor state results in the reduction of the electronic conductivity. Consequently, when the temperature is raised from 500 °C to 700 °C, the electronic conductivity of $Y_1Ba_2Cu_3O_{7-\delta}$ is reduced. Because the rate of the charge transfer reaction (i.e., $O + 2e^- + V_{\ddot{O}} \rightarrow O_O^x$) in the oxygen reduction process is proportional to the electronic conductivity of the electrode [19], the reduction of the electronic conductivity decreases the activity of the oxygen reduction. On the other hand, Pt is always in a metallic state. This may explain why the cathodic performance of $Y_1Ba_2Cu_3O_{7-\delta}$ becomes worse than that of Pt as the temperature is raised from 500 °C to 700 °C.

According to the above results and discussion, the electrical property of $Y_1Ba_2Cu_3O_{7-\delta}$ at 500 °C is similar to that of Pt, both being in a metallic state. Thus, the difference in cathodic performance between $Y_1Ba_2Cu_3O_{7-\delta}$ and Pt, as shown in Fig. 2, may not be attributed to the electrical property. It is proposed that this difference is attributed to the topography of the charge-exchange region. The triple-phase boundary, i.e., the three-phase interface of gas, electrode, and electrolyte, is the electrochemical reaction region for carrying out the charge transfer reaction. It has been demonstrated that mixed conductors such as LaSrMO (M = Co,Mn,Fe) can provide their whole surface as the triple-phase boundary [9, 10, 20]. As reported in many investigations [1, 4–6, 21–23], $Y_1Ba_2Cu_3O_{7-\delta}$ is a mixed conductor. Hence, the whole surface of the $Y_1Ba_2Cu_3O_{7-\delta}$ electrode can be used as the electrochemical reaction site. In contrast, since Pt is only an electronic conductor, its triple-phase boundary is only at the interface of electrode and electrolyte. It is clear that the electrochemical reaction region of the $Y_1Ba_2Cu_3O_{7-\delta}$ electrode is much larger than that of the Pt electrode. This may be the reason why the cathodic performance of $Y_1Ba_2Cu_3O_{7-\delta}$ is better than that of Pt at 500 °C.

From the above discussion, the delocalization of the triple-phase boundary from the electrode-electrolyte interface to the whole electrode surface is proposed as an important function for the $Y_1Ba_2Cu_3O_{7-\delta}$ material when used as a cathode for SOFCs. Recently, it was reported that $Ce_{0.9}Gd_{0.1}O_{1.95}$ is adequate as an electrolyte in SOFC for 500 °C operation [24]. This provides a significant impetus to the development of $Y_1Ba_2Cu_3O_{7-\delta}$ as a cathode in SOFCs which employ $Ce_{0.9}Gd_{0.1}O_{1.95}$ as the electrolyte for low-temperature operations.

Dependence of cathodic behavior of $Y_1Ba_2Cu_3O_{7-\delta}$ on oxygen concentration

The relationships between the cathodic current-overpotential curves and the oxygen concentration are shown in Figs. 4–6. Comparing Fig. 4 with Fig. 5 and Fig. 6, it is found that the dependence of the oxygen reduction rate over $Y_1Ba_2Cu_3O_{7-\delta}$ on oxygen concentration at 500 °C is much less than that at 700 °C and 800 °C. This indicates that the oxygen adsorption step, whose rate is closely related to the oxygen concentration, is not the major cause of resistance to the oxygen reduction process at 500 °C.

In contrast to the situation at 500 °C, at temperatures equal to and above 700 °C, oxygen concentration strongly influences the activity of the oxygen reduction

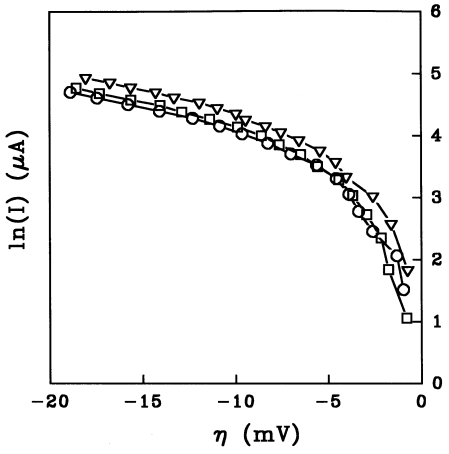

Fig. 4 Current-overpotential curves for YBCO electrode at 500 °C with different P_{O_2} values; *circle symbol* 2.5×10^{-3} atm; *square symbol* 5×10^{-3} atm; *triangle symbol* 1.5×10^{-2} atm

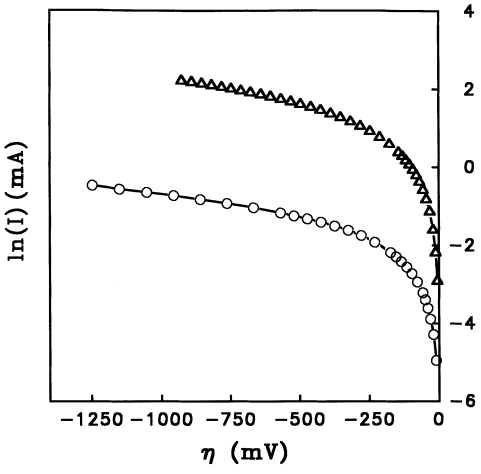

Fig. 5 Current-overpotential curves for YBCO electrode at 700 °C with different P_{O_2} values; *circle symbol* 10^{-4} atm; *triangle symbol* 10^{-2} atm

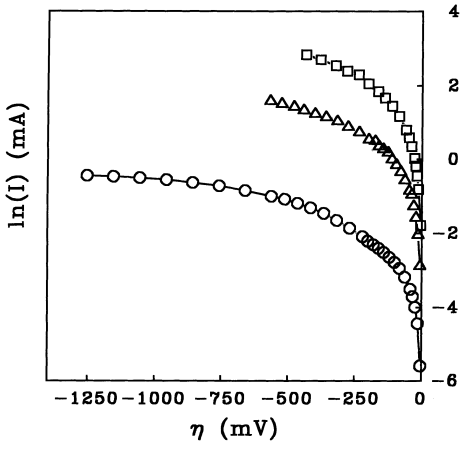

Fig. 6 Current-overpotential curves for YBCO electrode at 800 °C with different P_{O_2} values; *circle symbol* 10^{-4} atm; *triangle symbol* 10^{-2} atm; *square symbol* 0.21 atm

on $Y_1Ba_2Cu_3O_{7-\delta}$, as shown in Figs. 5 and 6. This means that at elevated temperatures (i.e., above 700 °C), the resistance to oxygen reduction is probably due to oxygen adsorption. In addition, as also shown in Figs. 5 and 6, the limiting current which is due to surface-diffusion control, does not appear even at very high overpotentials. In contrast, as can be seen from Fig. 7, on a Pt electrode, the limiting current occurs at relatively low overpotentials. This means that, at elevated temperatures, surface diffusion on the $Y_1Ba_2Cu_3O_{7-\delta}$ electrode is not the rate-limiting step for the oxygen reduction process. On the other hand, according to the BET measurements, the $Y_1Ba_2Cu_3O_{7-\delta}$ electrode has a low surface area, namely around 1 m^2/g. In the studies of an LaSrMnO cathode by AC impedance, it was demonstrated [20] that the rate-limiting step for oxygen reduction on the low-surface LaSrMnO is the oxygen adsorption step.

According to the above results and discussion, it is proposed that, at elevated temperatures (i.e., above 700 °C), oxygen adsorption on the $Y_1Ba_2Cu_3O_{7-\delta}$ electrode provides the major resistance to oxygen reduction. In order to prove this hypothesis, two specific electrodes with structures of $Pt/Y_1Ba_2Cu_3O_{7-\delta}$ and $Ag/Y_1Ba_2Cu_3O_{7-\delta}$ were designed and employed to study the behavior of oxygen adsorption. The $Y_1Ba_2Cu_3O_{7-\delta}$ electrode is coated with a layer of porous Pt or Ag, which is a catalyst with strong oxygen chemisorption. As shown in Fig. 8, compared to the $Y_1Ba_2Cu_3O_{7-\delta}$ electrode, the cathodic overpotential is largely decreased by using $Pt/Y_1Ba_2Cu_3O_{7-\delta}$ or $Ag/Y_1Ba_2Cu_3O_{7-\delta}$ as the cathode. This result is in accord with the above conclusion that the oxygen adsorption step provides the main resistance to oxygen reduction. On the other hand, because $Y_1Ba_2Cu_3O_{7-\delta}$ is coated with a layer of Pt or Ag, the distance for the oxygen diffusion from the electrode surface to the triple-phase boundary increases and the cathodic overpotential should thus increase. However, as shown in Fig. 8, the cathodic polarization is improved instead. Thus, it is also demonstrated that

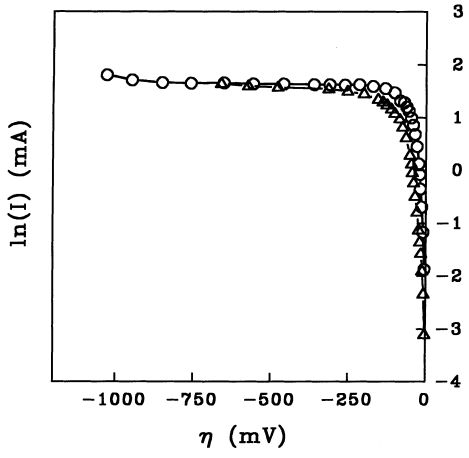

Fig. 7 Current-overpotential curves for Pt electrode at $P_{O_2} = 10^{-4}$ atm; *triangle symbol* 700 °C; *circle symbol* 800 °C

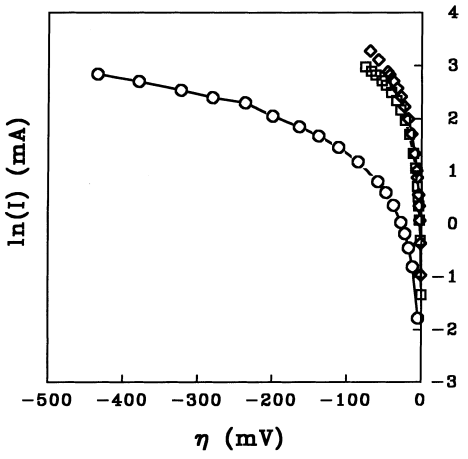

Fig. 8 Current-overpotential curves at 800 °C and $P_{O_2} = 0.21$ atm; *circle symbol* YBCO electrode; *square symbol* Pt/YBCO electrode; *diamond symbol* Ag/YBCO electrode

the probability that the oxygen surface diffusion is the rate-limiting step can be excluded. Further, based on the above experimental results, the mechanism is verified by an electrochemical model and mathematical simulation in the next section.

Oxygen reduction mechanism at elevated temperature

The oxygen reduction path on the $Y_1Ba_2Cu_3O_{7-\delta}$ (YBCO) cathode is shown in Fig. 1. The reaction mechanism is considered to be the following:

$$O_2 + * \rightarrow O_2* \tag{1}$$

$$O_2* + * \rightarrow 2O* \tag{2}$$

$$O*_{(s)} \xrightarrow{\text{surface diffusion}} O^*_{(v)} \tag{3}$$

$$O*_{(v)} + 2e^-_{(YBCO)} + V_{\ddot{O}_{(YBCO)}} \rightarrow O_{O^x_{(YBCO)}} \tag{4}$$

$$O_{O^x_{(YBCO)}} \xrightarrow{\text{migration}} \text{YBCO-YSZinterface} \tag{5}$$

Steps 4 and 5 show that $Y_1Ba_2Cu_3O_{7-\delta}$ is regarded as a mixed conductor of electron and oxygen ion. Several investigations [3, 21, 23] into the oxygen ionic conductivity of $Y_1Ba_2Cu_3O_{7-\delta}$ have indicated that the conductivity at 800 °C is around 6×10^{-3} $(\Omega\ \text{cm})^{-1}$ and is two orders of magnitude greater than that at 500 °C. Thus, in this work, the above oxygen reduction mechanism is discussed at temperatures equal to and above 700 °C.

The current-overpotential relation [25] can be expressed as

$$I = I_o\left[\frac{C_O}{C_{O_{(eq)}}} e^{-\alpha n f \eta} - \frac{C_{Oo^x}}{C_{Oo^x_{(eq)}}} e^{(1-\alpha) n f \eta}\right] \tag{6}$$

Earlier investigations usually assume that the term of oxygen-ion concentration, i.e., $C_{Oo^x}/C_{Oo^x_{(eq)}}$, is equal to unity [26, 27]. This indicates that the influence of the oxygen-ion migration rate on the oxygen reduction rate has not yet been explored. In this work, we apply Gauss's law and the Nernst equation to express the oxygen-ion concentration as a function of overpotential and current so as to clarify this influence.

According to the above analysis of the current-overpotential characteristics of $Y_1Ba_2Cu_3O_{7-\delta}$, it is proposed that the oxygen adsorption step (1) is the rate-limiting step for oxygen reduction. The adsorption rate of oxygen molecule is expressed as [28]

$$I = r_a = k_a P_{O_2}(1 - \theta_{O_2} - \theta_O) \tag{7}$$

When oxygen adsorption is rate limiting, the oxygen dissociation step (2) can be considered to be at an equilibrium state. Thus, according to the Langmuir isotherm [28],

$$(1 - \theta_{O_2} - \theta_O)\theta_{O_2} = K(\theta_O)^2 \tag{8}$$

From Eq. 8, we can get

$$1 - \theta_{O_2} - \theta_O = \frac{1 - \theta_O}{2} \pm \frac{\sqrt{1 - 2\theta_O + (1 - 4K)(\theta_O)^2}}{2} \tag{9}$$

Assume the square root item in Eq. 9 approaches zero, which will be identified by final simulation results.

Hence,

$$1 - \theta_{O_2} - \theta_O = \frac{1 - \theta_O}{2} \tag{10}$$

Substituting Eq. 10 into Eq. 7, we get

$$I = k_a P_{O_2} \frac{1 - \theta_O}{2} \tag{11}$$

If θ_O is substituted for the term of $C_O/C_{O_{(eq)}}$ in Eq. 6 [29], then Eq. 6 becomes

$$I = I_O\left\{\left(1 - \frac{2I}{k_a P_{O_2}}\right) e^{-\alpha n f \eta} - \frac{C_{Oo^x}}{C_{Oo^x_{(eq)}}} e^{(1-\alpha) n f \eta}\right\} \tag{12}$$

The oxygen-ion concentration, C_{Oo^x}, can be correlated with the electric potential by the migration step (5). The migration rate of oxygen anion through oxygen vacancy under an electric field for one dimension can be expressed as [30]

$$I = zeB_m C_{Oo^x}\left|\frac{\partial \phi}{\partial x}\right| \tag{13}$$

This application of Eq. 13 means that the oxygen reduction rate is related to oxygen-ion migration. Moreover, in the following discussion, it will be shown that the influence of the oxygen-ion migration rate on the rate of the oxygen reduction process is important only at low overpotentials.

The value of $C_{\mathrm{Oo}^{x}_{(\mathrm{eq})}}$, which is the oxygen-ion concentration at an equilibrium state, can be obtained by the Nernst equation [25],

$$E_{\mathrm{eq}} = E^{\mathrm{o}'} + \frac{RT}{nF}\ln\frac{C_{\mathrm{O}_{(\mathrm{eq})}}}{C_{\mathrm{Oo}^{x}_{(\mathrm{eq})}}} \tag{14}$$

Using Eqs. 13 and 14, Eq. 12 can be rewritten as

$$I = I_{\mathrm{o}}\left\{\left(1-\frac{2I}{k_{\mathrm{a}}P_{\mathrm{O}_2}}\right)\mathrm{e}^{-\alpha nf\eta} - \frac{\mathrm{e}^{-nfE^{\mathrm{o}'}}}{C_{\mathrm{O}_{(\mathrm{eq})}}}\frac{I}{zeB_m}\frac{1}{|\partial\phi/\partial x|}\mathrm{e}^{nfE_{\mathrm{eq}}}\mathrm{e}^{(1-\alpha)nf\eta}\right\} \tag{15}$$

By Gauss's law [31], we can correlate the electric field $(\partial\phi/\partial x)$ with the overpotential (η). According to the Poisson equation [31],

$$\frac{\partial^2\phi}{\partial x^2} = -\frac{\rho}{\varepsilon_{\mathrm{o}}}$$

When there is no net charge inside a closed surface, we obtain

$$\frac{\partial^2\phi}{\partial x^2} = 0$$

and

$$\frac{\partial\phi}{\partial x} = \text{constant}$$

This equation shows that the change of the electric field in a thin film of electrode is linear. Therefore, the term $\left|\frac{\partial\phi}{\partial x}\right|$ in Eq. 15 can be assumed as $\left|\frac{\eta}{L}\right|$. Substituting $\left|\frac{\eta}{L}\right|$ for $\left|\frac{\partial\phi}{\partial x}\right|$, Eq. 15 can be rewritten as

$$I = I_{\mathrm{o}}\frac{\mathrm{e}^{-\alpha nf\eta}}{1 + A(P_{\mathrm{O}_2})\mathrm{e}^{-\alpha nf\eta} + B\frac{1}{|\eta|}\mathrm{e}^{nfE_{\mathrm{eq}}}\mathrm{e}^{(1-\alpha)nf\eta}} \tag{16}$$

where

$$A = \frac{2}{k_{\mathrm{a}}}, B = \frac{\mathrm{e}^{-nfE^{\mathrm{o}'}}LI_{\mathrm{o}}}{zeB_mC_{\mathrm{O}_{(\mathrm{eq})}}}$$

The parameter A is related to oxygen adsorption and the parameter B is related to oxygen-ion migration. Equation 16 represents the assumption that the rate-limiting step of the oxygen reduction process is oxygen adsorption on the $Y_1Ba_2Cu_3O_{7-\delta}$ electrode.

At low overpotentials, since there is little resistance due to oxygen surface diffusion, the term $(C_{\mathrm{O}}/C_{\mathrm{O}_{(\mathrm{eq})}})$ in

Table 1 The values of parameters A and B

	700 °C		800 °C	
	10^{-2} atm	0.21 atm	10^{-2} atm	0.21 atm
A	0.0747	0.0827	0.1078	0.0841
B	0.1805	0.0451	0.1838	0.0443

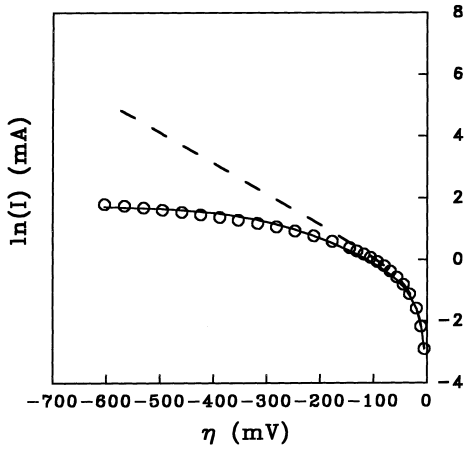

Fig. 9 Current-overpotential curves for YBCO electrode at 700 °C and $P_{\mathrm{O}_2} = 10^{-2}$ atm; *circle symbol* experimental data; *solid line* calculated from Eq. 16; *dash line* calculated from Eq. 18

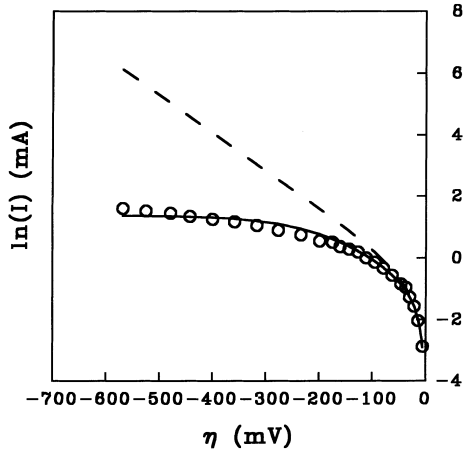

Fig. 10 Current-overpotential curves for YBCO electrode at 800 °C and $P_{\mathrm{O}_2} = 10^{-2}$ atm; *circle symbol* experimental data; *solid line* calculated from Eq. 16; *dash line* calculated from Eq. 18

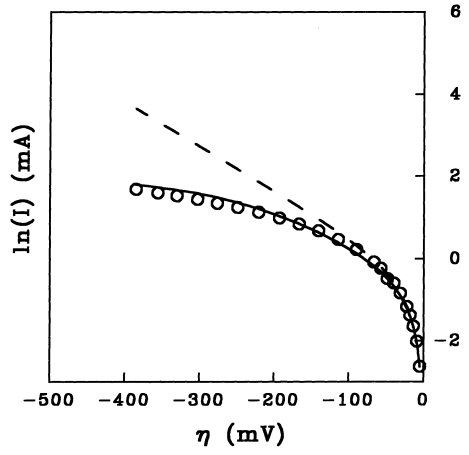

Fig. 11 Current-overpotential curves for YBCO electrode at 700 °C and $P_{\mathrm{O}_2} = 0.21$ atm; *circle symbol* experimental data; *solid line* calculated from Eq. 16; *dash line* calculated from Eq. 18

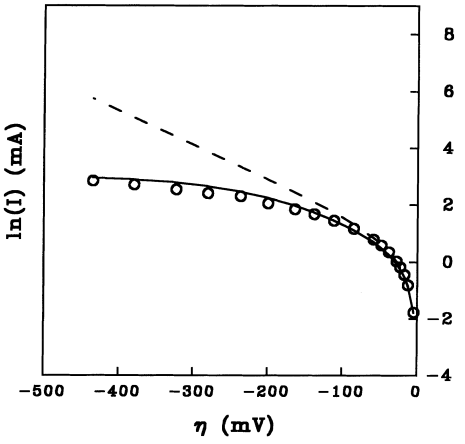

Fig. 12 Current-overpotential curves for YBCO electrode at 800 °C and $P_{O_2} = 0.21$ atm; *circle symbol* experimental data; *solid line* calculated from Eq. 16; *dash line* calculated from Eq. 18

Eq. 6 can be assumed to be equal to unity [25]. Equation 6 is thus simplified to

$$I = I_o \left[e^{-\alpha n f \eta} - \frac{C_{Oo^x}}{C_{Oo^x_{(eq)}}} e^{(1-\alpha) n f \eta} \right] \tag{17}$$

This equation shows that the rate of oxygen reduction is closely related to the oxygen-ion concentration. Hence, at low overpotentials, the oxygen-ion migration step (5) is assumed to be the rate-limiting step for oxygen reduction. The term $C_{Oo^x}/C_{Oo^x_{(eq)}}$ in Eq. 17 is treated by the same method as for of deriving Eq. 16, and thus Eq. 17 becomes

$$I = I_o \frac{e^{-\alpha n f \eta}}{1 + B \frac{1}{|\eta|} e^{n f E_{eq}} e^{(1-\alpha) n f \eta}} \tag{18}$$

The parameters A and B in Eqs. 16 and 18 as calculated from the current-overpotential data at different temperatures and oxygen pressures are shown in Table 1.

The simulation results for the cathodic characteristics are shown in Figs. 9–12. At low overpotentials (i.e., $|\eta| < 100$ mV), the experimental data correspond to the theoretical values as calculated by Eqs. 16 and 18. This means that, at low overpotentials, the resistance of the oxygen reduction process comes from both the oxygen adsorption step and the oxygen-ion transport step.

On the other hand, at high overpotentials (i.e., $|\eta| > 100$ mV), the experimental data can be fitted only by Eq. 16. Moreover, according to the calculation from experimental data, at high overpotentials(i.e., $|\eta| > 100$ mV),

$$A(P_{O_2}) e^{-\alpha n f \eta} \gg B \frac{1}{|\eta|} e^{n f E_{eq}} e^{(1-\alpha) n f \eta} \tag{19}$$

This shows that the influence of oxygen-ion migration on oxygen reduction is not important at high overpotentials (i.e., $|\eta| > 100$ mV). Hence, at high overpotentials, the influence of oxygen adsorption on oxygen reduction is much greater than that of oxygen-ion migration. This result is in accord with the experimental data. It is thus concluded that oxygen adsorption provides the greatest resistance to oxygen reduction on a $Y_1Ba_2Cu_3O_{7-\delta}$ electrode at high overpotentials. At the same time, the assumption that the square root term in Eq. 9 approaches zero is reasonable because the simulation results shown in Figs. 9–12 are very consistent with experimental data.

Conclusion

Delocalization of the triple-phase boundary is proposed as an important function of $Y_1Ba_2Cu_3O_{7-\delta}$ used as the cathode in SOFCs. The results of mathematical simulation with oxygen adsorption as the rate-limiting step show good agreement with the experimental data. Moreover, a layer of strong oxygen-adsorption catalyst such as Pt or Ag deposited over the $Y_1Ba_2Cu_3O_{7-\delta}$ electrode improves the cathodic polarization. Therefore, it is concluded that the major resistance to oxygen reduction on $Y_1Ba_2Cu_3O_{7-\delta}$ is from the oxygen adsorption step.

Acknowledgement This work was supported by the National Science Council of the Republic of China under contract No. NSC-81-0402-E-007-09.

References

1. Nelson DL, Whittingham MS, George TF (1987) Chemistry of high-temperature superconductors. American Chemical Society, Washington
2. Kishio K, Shimoyama J, Hasegawa T, Kitazawa K, Fueki K (1987) Jpn J Appl Phys 26: L1228
3. Turrillas X, Kilner JA, Kontoulis I, Steele BCH (1989) J Less Comm Met 151: 229
4. Islam MS (1990) Supercond Sci Technol 3: 531
5. Baikov YM, Shalkova EK, Vshakova TA (1993) Supercond Phys Chem Technol 36(3): 349
6. Grader GS, Gallagher PK, Thomson J, Gurvitch M (1988) Appl Phys A 45: 179
7. Kinoshita K (1992) Electrochemical oxygen technology. Wiley, New York
8. Haart LGJ, Kuipers RA, Vries KJ, Burggraaf AJ (1991) J Electrochem Soc 138: 1970
9. Siebert E (1994) Electrochim Acta 39: 1621
10. Gharbage B, Pagnier T, Hammou A (1994) J Electrochem Soc 141: 2118
11. Takeda Y, Kanno R, Noda M, Tomida Y, Yamamoto O (1987) J Electrochem Soc 134: 2656
12. Poole CP, Datta T, Farach HA (1988) Copper oxide superconductors. Wiley, New York
13. Bi YJ, Wellhofer F, Day MJ, Abell JS (1993) Mat Sci Eng B21: 19
14. Chang CL, Huang TJ (1995) I & EC Research 34: 2364
15. Pickett WE, Cohen RE, Krakauer H (1990) Phys Rev B42: 88764 (1990)
16. Rao CNR (1991) Chemistry of high temperature superconductors. World Scientific, New Jersey
17. Kishio K, Shimoyama J, Hasegawa T, Kitazawa K, Fueki K (1987) Jpn J Appl Phys 26: L1228

18. Kittel C (1991) Introduction to solid-state physics. Wiley, New York
19. Tedmon CS, Spacil HS, Mitoff SP (1969) J Electrochem Soc 116:1170
20. Herle JV, McEvoy AJ, Thampi KR (1994) Electrochim Acta 39: 1675
21. Vischjager DJ, Zomeren AA, Schoonman J (1990) Solid State Ionics 40/41: 810
22. Kumar RV, Fray DJ, Evetts JE, Williams HW, Misson A (1993) J Electrochem Soc 140: 2893
23. MacManus JL, Fray DJ, Evetts JE (1992) Physica C 190: 2511
24. Steele BCH (1994) J Power Sources 49: 1
25. Bard AJ, Faulker LR (1980) Electrochemical Methods: Fundamentals and Applications. Wiley, New York
26. Nguyen BC, Rincon-Rubio LM, Mason DM (1986) J Electrochem Soc 133: 1860
27. Kenjo T, Horiuchi Y, Osawa S (1990) J Electrochem Soc 137: 2423
28. Satterfield CN (1980) Heterogeneous Catalysis in Practice. McGraw-Hill, New York
29. Wang DY, Nowick AS (1979) J Electrochem Soc 126: 1155
30. Rickert H (1982) Electrochemistry of Solids. Springer, Berlin Heidelberg New York
31. Feynman RP, Leighton RB, Sands M (1964) Lectures on Physics. Addison-Wesley, New York